

## Jet-environment interactions in FRI radio galaxies

R.A. Laing

*ESO, Karl-Schwarzschild-Straße 2, 85748 Garching-bei-München,  
Germany*

A.H. Bridle

*NRAO, 520 Edgemont Road, Charlottesville, VA 22903-2475, U.S.A.*

**Abstract.** There is now unequivocal evidence that the jets in FR I radio galaxies are initially relativistic, decelerating flows. On the assumption that they are axisymmetric and intrinsically symmetrical (a good approximation close to the nucleus), we can make models of their geometry, velocity, emissivity and field structure whose parameters can be determined by fitting to deep VLA observations. Mass entrainment – either from stellar mass loss within the jet volume or via a boundary layer at the jet surface – is the most likely cause for deceleration. This idea is quantitatively consistent with the velocity field and geometry inferred from kinematic modelling and the external gas density and pressure profiles derived from X-ray observations. The jets must initially be very light, perhaps with an electron-positron composition.

### 1. Introduction

The morphological division of extragalactic radio sources into two classes introduced by Fanaroff & Riley (1974) has proved to be remarkably robust. Fanaroff & Riley had already noted that the edge-brightened (FR II) sources tend to have higher radio luminosities than the edge-darkened (FR I) sources, but there is also a dependence on stellar luminosity of the host galaxy which makes the division even cleaner (Ledlow & Owen 1996). That said, the FRI class is not homogeneous: examples of the range of structures are shown in Fig. 1. Although almost all FRI sources show jets on small scales, some appear to be confined to the nuclear regions (e.g. 3C 84; Fig. 1a) while others persist almost to the outer edges of the source structure (e.g. 3C 296; Fig. 1f).

It has long been surmised (e.g. Simon 1978; Fanti et al. 1982) that the characteristic structures of FRI sources result from deceleration and disruption of their jets, perhaps triggered by interaction with the surrounding intergalactic medium. Turning this perception from a vague idea into a quantitative description of source dynamics proved to be a slow process, but significant progress has recently been made using a combination of deep radio imaging, sophisticated jet modelling and an understanding of the external environments of the sources from X-ray observations. These results bear on five of Blandford (2007)'s tasks: map jet velocity fields; understand the changing composition; measure jet pressures; deduce jet confinement mechanisms and infer jet powers and thrusts.

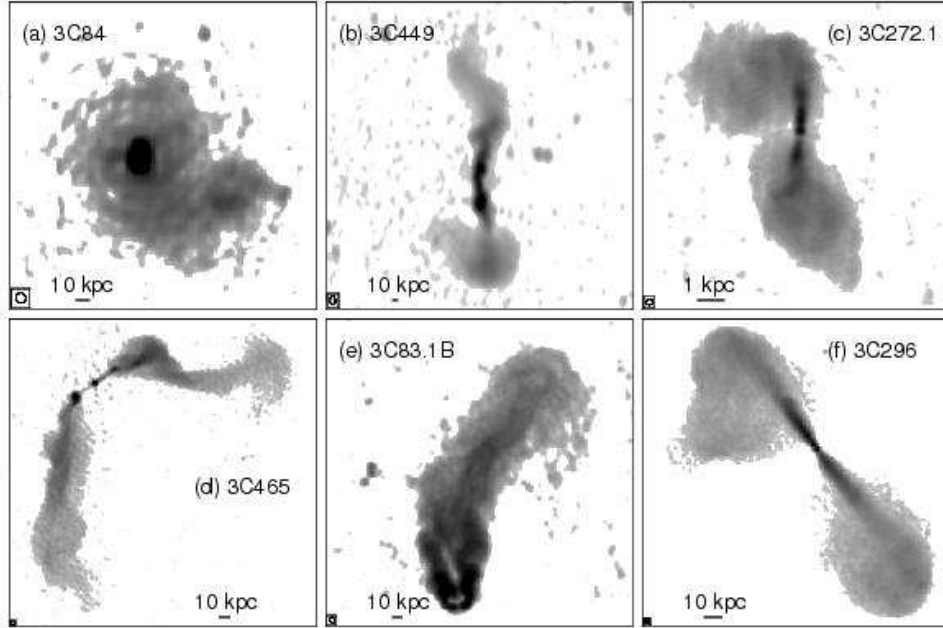


Figure 1. Examples of the radio structures of FRI sources from the 3CRR catalogue (Leahy, Bridle & Strom 2000).

## 2. FRI jets as decelerating, relativistic flows

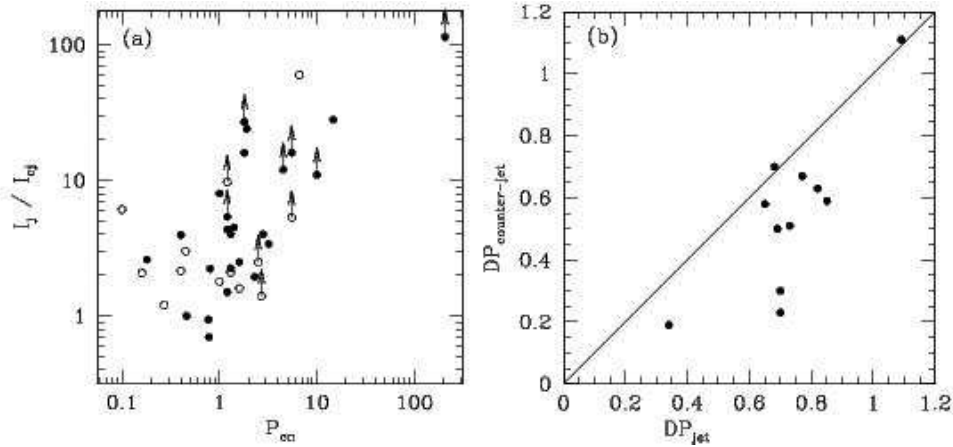


Figure 2. (a) A plot of jet/counter-jet intensity ratio at the brightening point,  $I_j/I_{cj}$ , against normalized core power,  $P_{CN}$  for sources from the B2 sample (Laing et al. 1999). (b) Depolarization on the counter-jet ( $DP_{\text{counter-jet}}$ ) and jet ( $DP_{\text{jet}}$ ) sides for sources from the same sample with  $I_j/I_{cj} > 4$  (Morganti et al. 1997).

Deceleration of a symmetric, initially relativistic flow provides a very natural explanation for the decrease in jet/counter-jet sidedness ratio  $I_j/I_{cj}$  with

distance from the nucleus observed in FRI jets (e.g. Laing 1993). There is now direct evidence for relativistic motions of jet knots on kpc scales in M87 and Cen A (Biretta, Zhou & Owen 1995; Harris et al. 2007; Hardcastle et al. 2003) and many other results are mostly easily explained if FRI jet bases are relativistic. For example,  $I_j/I_{cj}$  is correlated with core fraction (Laing et al. 1999, Fig. 2a) and the counter-jet lobe depolarizes more rapidly with increasing wavelength than that associated with the brighter jet (Morganti et al. 1997, Fig. 2b).

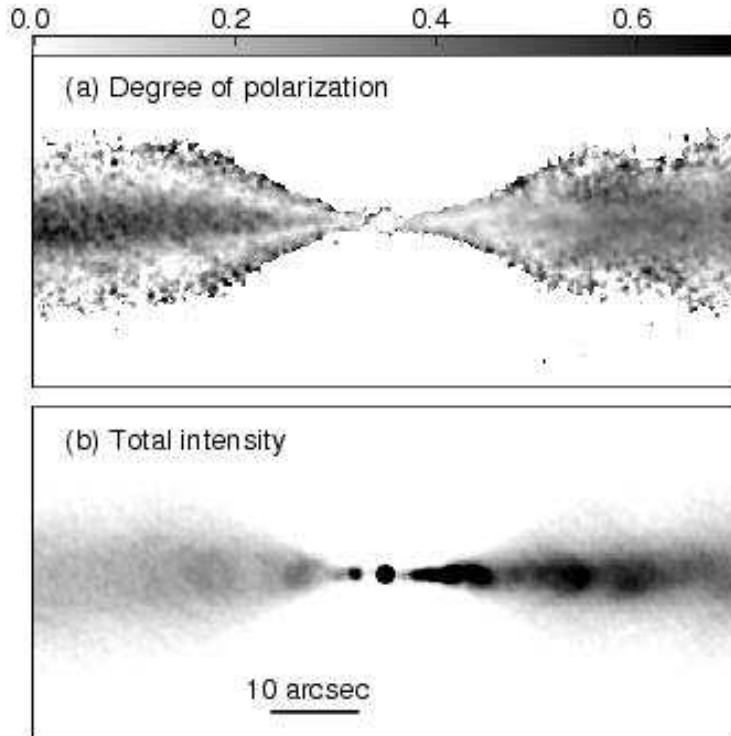


Figure 3. Images of 3C 296 at a resolution of 0.75 arcsec (Laing et al. 2006). (a) degree of polarization; (b) total intensity.

An example of the characteristically asymmetric appearance of FRI jet bases is shown in Fig. 3(b). As well as this asymmetry, the main and counter-jets also show differences in their transverse brightness profiles, in the sense that the main jet is more centrally peaked (e.g. Fig. 4). This is a natural manifestation of a transverse velocity gradient, with higher flow speeds on-axis. There is also a systematic difference in polarization structure between the main and counter-jets (e.g. Fig. 3a), in the sense that the brighter jet base has a smaller degree of polarization on-axis with more prominent regions of longitudinal apparent magnetic field. If the jets are intrinsically symmetric and relativistic, this effect must be due to aberration, which causes the two jets to be observed at different angles to the line of sight in the rest frames of their emitting material and therefore to have different observed polarizations. The combination of asymmetries in total intensity and linear polarization provides enough information to break the degeneracy between flow velocity and angle to the line of

sight, as well as to constrain the three-dimensional structure of the magnetic field, allowing us to make detailed models of the jets.

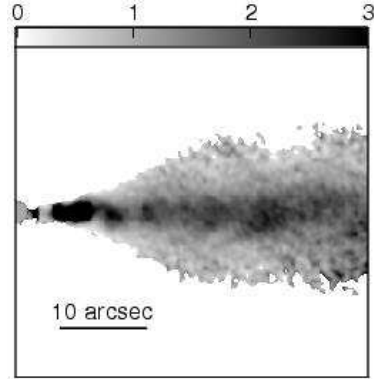


Figure 4. Jet sidedness for 3C 296, derived by dividing the total-intensity image from Fig. 3(b) by a copy of itself rotated by  $180^\circ$  (Laing et al. 2006).

### 3. Models of FRI jets: geometry, speed and field structure

We have now modelled the flows in five FRI radio galaxies: 3C 31, B2 0326+39, B2 1553+24, NGC 315 and 3C 296 (Laing & Bridle 2002a; Canvin & Laing 2004; Canvin et al. 2005; Laing et al. 2006). We assume that the jets are precisely symmetrical, axisymmetric, relativistic flows and derive their geometries, velocity fields, emissivity and magnetic-field component ratios by fitting to deep VLA observations. We find that a decelerating jet model fits the observed brightness and polarization structures and asymmetries well (e.g. Fig. 5).

FRI jets on kpc scales can generally be divided into a flaring region (where the expansion rate first increases rapidly and then decreases again) and an outer region in which the expansion is uniform. We cannot model the jets within a kpc or so of the nucleus, where they tend to be faint and poorly resolved by the VLA. Where they first brighten, we derive characteristic on-axis velocities  $\beta = v/c \approx 0.8$ . Rapid deceleration then occurs over distances of 1 – 10 kpc (always before the jets recollimate), after which the velocity either stays constant or decreases less rapidly. For all sources except 3C 296, the transverse velocity profiles are consistent with edge/on-axis ratios  $\approx 0.7$  everywhere (although we cannot rule out evolution from a top-hat profile at the initial brightening). In 3C 296, the only source with a bridged twin-jet structure that we have observed in sufficient detail (Fig. 1f), the velocity falls to a low fractional value  $\lesssim 0.1$  at the jet edge. The jets in 3C 296 may be embedded within the lobes rather than propagating in direct contact with the interstellar medium of the host galaxy, as appears to be the case for the other sources. Velocity fields for four of the sources are shown in Fig. 6.

The data hint at further complexity in the jet velocity fields before the initial brightening. Measurements of both sidedness ratio and proper motion on pc scales in NGC 315 indicate an apparent *acceleration* (Cotton et al. 1999, Fig. 7). Our VLA observations also show slightly smaller sidedness ratios in the

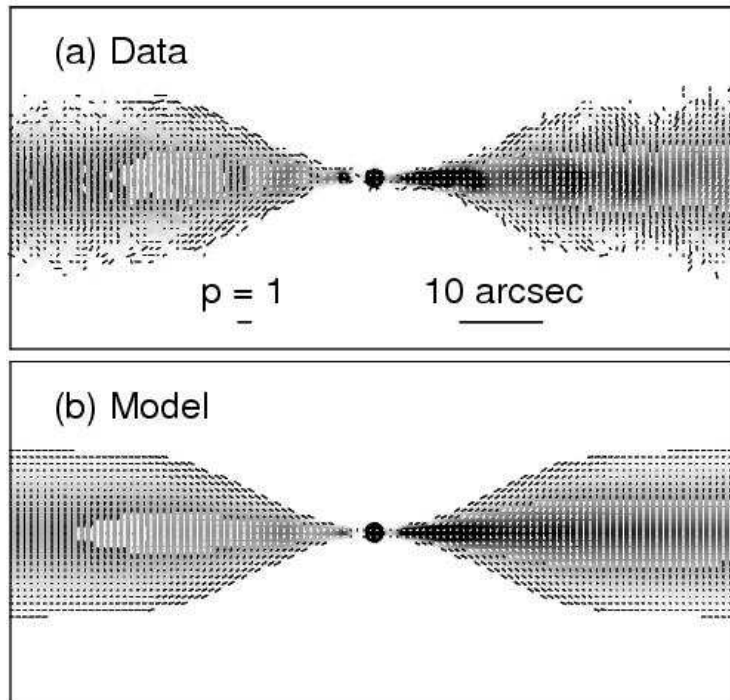


Figure 5. A comparison between data and model for 3C 296 (Laing et al. 2006). Vectors with magnitudes proportional to the degree of polarization,  $p$  and with directions along the apparent magnetic field are superimposed on grey-scales of total intensity. (a) Data; (b) model.

faint, kpc-scale jet bases than at or immediately after the brightening point for the four sources where we can resolve the former. If we observe a jet stratified in velocity with inadequate transverse resolution, the speed inferred for its *apparently* brightest emission will be influenced by how changes in its transverse emissivity profile interact with the (orientation-dependent) Doppler favouritism, and may give a misleading account of the true velocity variation along the jet. Both the pc-scale and faint kpc-scale regions are barely resolved in width, so we cannot yet tell whether the bulk flow really accelerates.

On average, the largest single magnetic-field component is toroidal. The longitudinal component is significant close to the nucleus but decreases with distance and the radial component is always the smallest of the three (e.g. Fig. 8). We also find that the toroidal component is stronger relative to the longitudinal component at the edge of the jet. The evolution of the field component ratios along the jets before they recollimate is not consistent with flux freezing in a laminar flow, which requires a much more rapid transition from longitudinal to transverse field than we infer. After recollimation, flux freezing is consistent with our results, however.

Before the jets decelerate and recollimate, the quasi-one-dimensional adiabatic approximation (together with flux freezing) is grossly inconsistent with the emissivity evolution inferred from our models. After deceleration and recol-

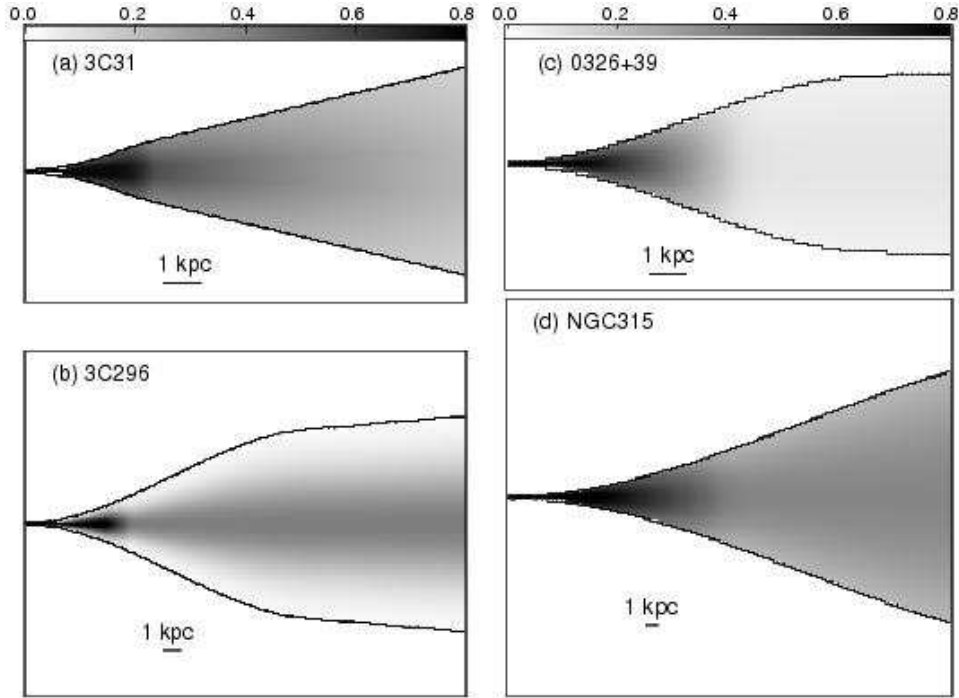


Figure 6. Grey-scales of jet speed derived from relativistic models for: (a) 3C 31 (Laing & Bridle 2002a); (b) 3C 296 (Laing et al. 2006); (c) B2 0326+39 (Canvin & Laing 2004); (d) NGC 315 (Canvin et al. 2005). The range is 0 –  $0.8c$ .

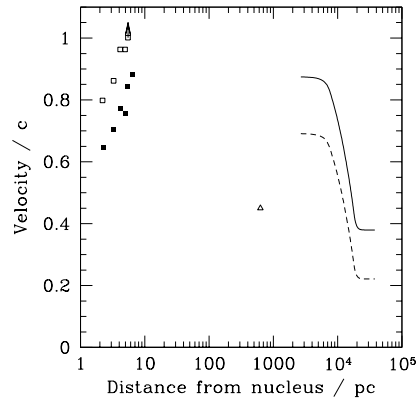


Figure 7. A comparison of velocity estimates for NGC 315 on pc and kpc scales, plotted against distance from the nucleus. Filled squares: velocities from proper motions; open squares: velocities from jet/counter-jet ratios (both from Cotton et al. 1999); open triangle: velocity derived from the jet/counter-jet ratio at 0.4 arcsec resolution close to the nucleus. The full and dotted lines show model fits for the centre and edge of the jets, respectively (Canvin et al. 2005).

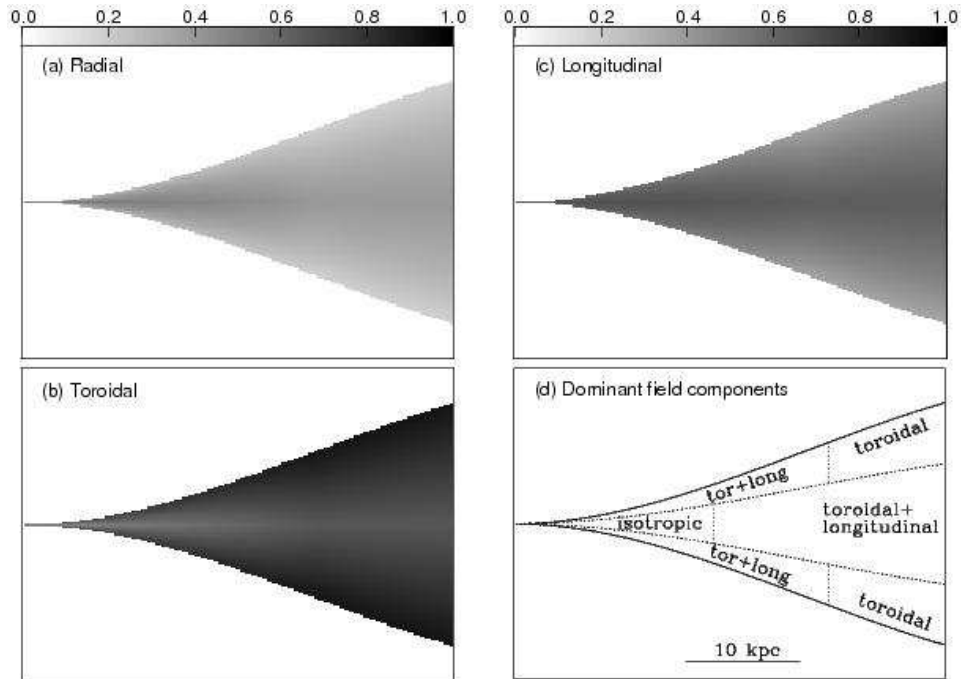


Figure 8. Grey-scales showing the fractional magnetic-components in the toroidal, longitudinal and radial directions inferred for the jets of NGC 315 by Canvin et al. (2005). The dominant components are sketched in panel (d).

limation, however, this approximation describes the emissivity evolution along the jets quite well. Details of the radio spectra and high-energy emission are given by Laing et al. (2007).

#### 4. Conservation-law analysis and jet energy fluxes

It is likely that FRI jets decelerate as a result of entraining matter, either by *injection* of mass lost from stars within the jet volume or by *ingestion* of ambient gas from the surrounding IGM via a mixing layer. The kinematic models of Section 3. prescribe the variation of velocity along a jet, together with its geometry. Given the external pressure and density profiles derived from X-ray observations, we can then apply conservation of energy, momentum and mass in the quasi-one-dimensional approximation, following Bicknell (1994) and including the effects of buoyancy. Two key assumptions are needed to close the problem: the jet is assumed to be in pressure equilibrium with the surrounding medium after recollimation and  $\Phi = \Pi c$ , as expected for an initially relativistic jet ( $\Phi$  is the energy flux with the rest-mass contribution subtracted and  $\Pi$  is the momentum flux). In addition, a relativistic equation of state is assumed and anisotropic magnetic stresses are neglected. The results of this calculation are estimates of the jet energy flux and the variations of internal pressure, density, mass flux and entrainment rate as functions of distance from the nucleus.

This technique was first applied to 3C 31 by Laing & Bridle (2002b). In Fig. 9 we also show the preliminary profiles of pressure, density, Mach number and entrainment rate for two other sources – B2 0326+39 and 3C 296 (Laing et al., in preparation). The top panels show the internal, external and synchrotron minimum pressures. By hypothesis, the first two are matched in the outer regions, but we also note that the pressure gradients are quite similar (for 3C 296 it is possible that the external pressure should be that of the lobe rather than the surrounding IGM). The synchrotron minimum pressure is comparable with or slightly less than the internal pressure in the outer parts, as expected if the latter is dominated by relativistic particles and fields close to equipartition. In all three sources, there is a significant overpressure at the brightening point (where the analysis starts) and this drives the initial expansion in the flaring region. The pressure becomes less than that of the surroundings at the end of the flaring region before the jet recollimates and reaches pressure equilibrium (the large under-pressure in B2 0326+39 between 2 and 4 kpc is probably due to an inaccurate estimate of the outer velocity, which is poorly constrained). The jet densities are very low (typically equivalent to 1 proton  $\text{m}^{-3}$ ), and the initial density ratios with the surroundings are  $\sim 10^{-5}$ . The jets are transonic, with Mach numbers  $\sim 1$ . The entrainment rate for 3C 31 continues to rise at large distances whereas the profiles for B2 0326+39 and 3C 296 both show peaks in the flaring region before dropping to very low values. The reason is that the kinematic model for 3C 31 requires continued deceleration after recollimation, whereas those for the other two sources indicate an approximately constant asymptotic velocity. Differences in external density and/or shielding by lobe material may be responsible. The entrainment rate profile for 3C 31 also shows a prediction for the mass input from stars in the jet volume (Laing & Bridle 2002b). This is comparable with the required entrainment rate close to the start of the model, but not at large distances, suggesting that mass injection and ingestion are both important.

The derived energy fluxes are  $\Phi \approx 1.1 \times 10^{37}$ ,  $7 \times 10^{36}$  and  $1.6 \times 10^{36}$  W, respectively, for 3C 31, 3C 296 and B2 0326+39. It will be of interest to compare these estimates with values derived from cavity dynamics (McNamara et al. 2007, and references therein). Estimates of the mass density and the number density of radiating electrons can be combined to constrain the composition of the jets (see Laing & Bridle 2002b for a detailed review of assumptions). At the brightening point, limiting cases include:

1. A power-law Lorentz-factor distribution  $n(\gamma)d\gamma \propto \gamma^{-2.2}d\gamma$  of relativistic electrons, each associated with a (cold) proton. In this case, there must be a low-energy cut-off at  $\gamma_{\min} \approx 35$  (3C 31 and B2 0326+39) or  $\approx 300$  (3C 296).
2. An electron-positron jet with entrained thermal matter providing essentially all of the mass.

Unfortunately, it is not yet possible to distinguish between these (and other) compositions.

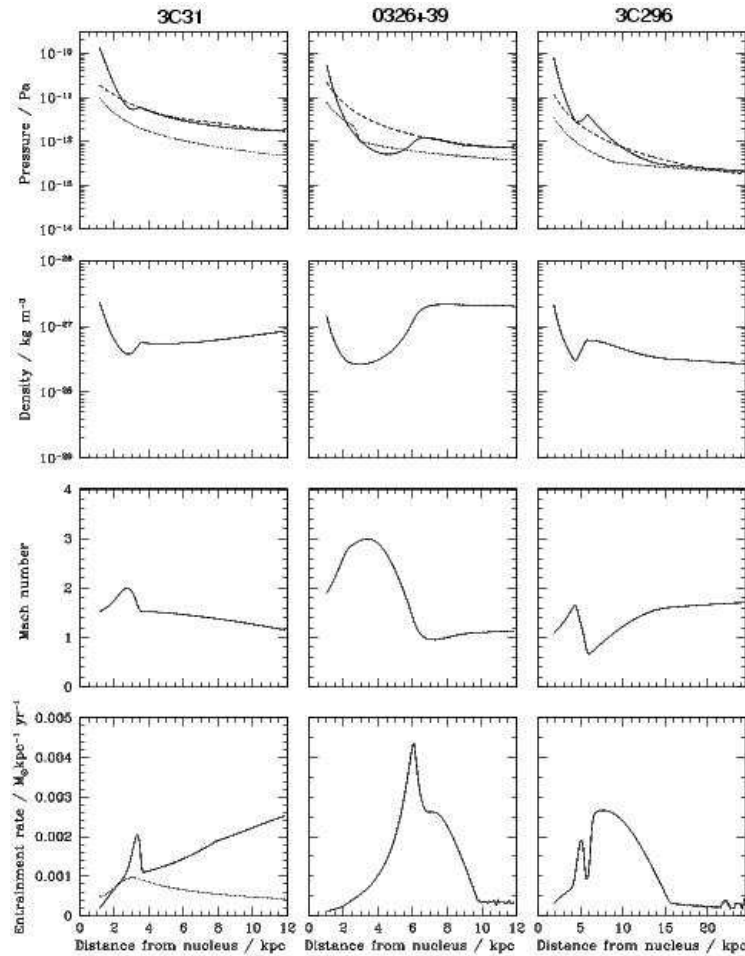


Figure 9. Profiles of pressure, density, Mach number and entrainment rate along the jets of 3C 31, B2 0326+39 and 3C 296 from a quasi-one-dimensional conservation-law analysis (Laing & Bridle 2002b, Laing et al., in preparation). In the pressure plots, the full, dashed and dotted lines show the internal, external and synchrotron minimum pressures, respectively. The dotted curve in the entrainment rate plot for 3C 31 is an estimate of mass input by injection from stars within the jet volume (Laing & Bridle 2002b).

## 5. Where next?

The techniques reviewed here have led to a detailed picture of the evolution of the FRI jets as they flare and decelerate. They work because we can compare both jets in the same source: sizes match the resolution of our most sensitive instruments, surface brightnesses are (just) high enough, Faraday rotation is easy to correct and jet speeds are modest. The key project when EVLA and eMERLIN become operational will be an attempt to apply the same methods to

other types of relativistic jet: closer to the launching scale and in FR II sources or microquasars. There are also more immediate questions, including:

1. What makes FR I jets brighten so abruptly in the radio band at distances of a few kpc from the nucleus?
2. Can we decide what combination of stellar mass-loss (injection) and external entrainment (ingestion) operates in FR I jets?
3. Can we (finally) detect internal depolarization and hence estimate densities of thermal matter now that we understand foreground Faraday screens much better?
4. Do different methods for estimating FR I jet powers (conservation-law, cavity dynamics, bow-shock physics) give the same answer? Can they be made consistent with radiation-loss timescales?
5. Do jets really accelerate on pc scales and/or as they flare or is this effect an artefact of inadequate transverse resolution?

**Acknowledgments.** The National Radio Astronomy Observatory is a facility of the National Science Foundation operated under cooperative agreement by Associated Universities, Inc.

## References

- Bicknell, G. V., 1994, *ApJ*, 422, 542  
 Biretta J.A., Zhou F., Owen F.N., 1995, *ApJ*, 447, 582  
 Blandford, R.D., these proceedings  
 Canvin, J.R., Laing, R.A., 2004, *MNRAS*, 350, 1342  
 Canvin, J.R., Laing, R.A., Bridle, A.H., Cotton, W.D., 2005, *MNRAS*, 363, 1223  
 Cotton W.D., Feretti L., Giovannini G., Lara L., Venturi T., 1999, *ApJ*, 519, 108  
 Fanaroff B.L., Riley J.M., 1974, *MNRAS*, 167, 31P  
 Fanti, R., Lari, C., Parma, P., Bridle, A.H., Ekers, R.D., Fomalont, E.B., 1982, *A&A*, 110, 169  
 Hardcastle M.J., Worrall D.M., Kraft R.P., Forman W.R., Jones C., Murray S.S., 2003, *ApJ*, 593, 169  
 Harris, D.E., Cheung, C.C., Stawarz, L., Biretta, J.A., Sparks, W., Perlman, E.S., Wilson, A.S., 2007, these proceedings  
 Laing, R.A., 1993, in Burgarella, D., Livio, M., O’Dea, C.P., eds, *Space Telescope Sci. Inst. Symp. 6: Astrophysical Jets*. Cambridge University Press, Cambridge, p. 95  
 Laing, R.A., Bridle, A.H., 2002a, *MNRAS*, 336, 328  
 Laing, R.A., Bridle, A.H., 2002b, *MNRAS*, 336, 1161  
 Laing, R.A., Canvin, J.R., Bridle, A.H., Hardcastle, M.J., 2006, *MNRAS*, 372, 510  
 Laing, R.A., Bridle, A.H., Cotton, W.D., Worrall, D.M., Birkinshaw, M., 2007, these proceedings  
 Laing, R.A., Parma, P., de Ruiter, H.R., Fanti, R., 1999, *MNRAS*, 306, 513  
 Leahy, J.P., Bridle, A.H., Strom, R.G., 2000, <http://www.jb.man.ac.uk/atlas>  
 Ledlow, M.J., Owen, F.N., 1996, *AJ*, 112, 9  
 McNamara, B.R., Birzan, L., Rafferty, D.A., Nulsen, P.E.J., Carilli, C., Wise, M.W., these proceedings  
 Morganti, R., Parma, P., Capetti, A., Fanti, R., de Ruiter, H.R., 1997, *A&A*, 326, 919  
 Simon, A.J.B., 1978, *MNRAS*, 184, 537